Journal of Mines, Metals and Fuels, *71(12A): 200-207; 2023. DOI: 10.18311/jmmf/2023/43612*

Print ISSN : 0022-2755

Journal of Mines, Metals and Fuels

Contents available at: *www.informaticsjournals.com/index.php/jmmf*

Structural and Dielectric Properties of $Cu_x Zn_{1-x} Fe_2O_4$ (x = 0.2, 0.6, 0.8) Nano Particles

Akash Daniel Georgi[1]*, Brian Jeevan Fernandes[2], G. Srinivas Reddy[3], K. P. Ramesh[2] and K. J. Mallikarjunaiah[1]

[1]Department of Physics, M. S. Ramaiah University of Applied Sciences, Bengaluru – 560058, Karnataka, India; akashgeorgi504@gmail.com, kjmarjun@gmail.com

[2]Department of Physics, Indian institute of Science, Bengaluru - 560012, Karnataka, India; brianf@iisc.ac.in, kpramesh@iisc.ac.in

[3]Department of Physics, School of Engineering, Presidency University, Bengaluru - 560089, Karnataka, India; gavinolasrinivasreddy@gmail.com

Abstract

Researchers widely investigate multi-ferrite nanoparticles due to their fascinating magnetic and electrical properties with satisfactory thermal and chemical stabilities. In the present work $Cu_xZn_{1-x}Fe_2O_4$(x = 0.2, 0.6, 0.8) were synthesized using the auto combustion method. The spinel structure of the prepared samples was verified using XRD. The compositional dependent dielectric and ac conductivity studies were performed using impedance spectroscopy technique. The dielectric properties, such as complex dielectric constant and impedance, have been studied as a function of frequency. Changes of dielectric loss tangent (tan δ) with the frequency have been studied to get information about the energy dispersed inside the materials. The ac conduction study, as a function of frequency, suggests the hopping conduction mechanism at the higher frequencies. From the complex impedance spectra (Nyquist plots or Cole-Cole plots), On the real axis, we identified a dispersion as opposed to a centered semicircle. This suggests a relaxation type other than Debye. The dielectric dispersion observed at lower frequencies can be explained using Koop's phenomenological theory. Since many gases are released during mining and the investigated $Cu_2Fe_2O_4$ is known to be an excellent gas sensor, this study helps to use it effectively in the mining sector.

Keywords: *Auto Combustion, Dielectric, Ferrites, Mining, Nyquist Plot*

1.0 Introduction

Spinel structure nano ferrites, with chemical formula MFe_2O_4, have intriguing magnetic and electric properties along with acceptable thermal and chemical stabilities, they are found to play a pivotal role in technical fields such as communication, medical, and electric fields[1]. Correspondingly multi-ferrite nanoparticles are widely investigated by researchers[2]. The mentioned properties are influenced by grain structure, inhomogeneities, presence of voids, surface layers and mainly occupancy of cations in the spinel structure[3]. These factors can be doctored through various aspects such as synthesize methods, sintering conditions and nature of divalent element[4]. It's noteworthy to know that ferrites can be synthesized through techniques such as co-precipitation, micro-emulsion, solid state reaction, sol-gel etc.

**Author for correspondence*

Spinel ferrite unit cell consists of 8 *fcc* cells of oxygen atom, containing 32 oxygen atoms, 16 iron and 8 divalent cations[5]. There are tetrahedral as well as octahedral sites in a spinel ferrite. Cation occupancy in these sites determine the type of spinel such as inverse, normal and mixed spinels. In inverse spinels Fe^{3+} ions occupy equally among tetrahedral and octahedral sites. In normal spinels Fe^{3+} ions occupy octahedral sites and divalent cation occupy tetrahedral sites. In mixed spinels divalent cations are distributed among both sites[6]. Zinc ferrite is known to exist as normal and copper ferrite crystallizes in inverse spinel structure[7].

One of the most serious environmental issues affecting the mining sector today is acid mine drainage, or AMD. The ground surface water that drains from a mining site where, sulfide minerals are treated is known as AMD. Sulfuric acid is created when sulfide minerals, especially pyrite and pyrrhotite, oxidize in water when exposed to oxygen. Other minerals are then leached by the acid[8]. Because of this, depending on the location, AMD has a range of metal pollutants. Wang *et al*[9]. has demonstrated that under ambient temperature conditions acid drainage solutions can be used to make spinel ferrites. The ability of the ferrite process to scavenge the majority of divalent metal ions and the precipitates that are produced to be stable and easily recovered by magnetic filtration are its two main benefits when treating AMD. A two-step continuous ferrite flow method for steady extraction from an actual AMD comprising copper, zinc, and arsenic was presented by Toshifumi *et al*[10]. Another reason to pursue the process is the potential commercial use of ferrite as recording media and magnetic indicators.

Dielectric properties refer to a material's ability to respond to an electric field. These properties are often characterized by parameters such as dielectric constant, dielectric loss, and electrical conductivity. In the case of $CuFe_2O_4$, its dielectric properties can be influenced by factors such as composition, crystal structure, and temperature. On the other hand, in underground mining, the air quality can be compromised by dust, fumes, and gases released during the extraction process. Gas sensors can monitor the air quality in real-time, providing information on pollutant levels and helps to implement measures to maintain a healthy working environment for miners[11,12]. Gas sensing involves the ability of a material to detect and respond to the presence of specific gases. The interaction between a gas and the sensing material leads to changes in electrical, optical, or other measurable properties. In gas sensing applications, $CuFe_2O_4$ has been explored for its response to various gases, including reducing gases like hydrogen and methane. The interaction between $CuFe_2O_4$ and gases can modulate its dielectric constant. Changes in the dielectric constant may occur as a result of gas-induced alterations in the electronic structure, charge distribution, or polarization of the material. This modulation can be exploited for gas sensing applications[13–15].

Besides this spinel ferrites cater for the applications of dielectric material owing to the tunability of the materials for the desired region of frequencies. Ferrites can be highly suitable for fabricating cores of transformers, high frequency applications and microwave absorption owing to its minimal dielectric loss and conductivity[7]. Hence engineering the material composition and tailoring the properties of the materials under study is important in knowing their suitability for the desired applications. In particular, dielectric behavior is one of the significant areas of ferrites to be studied due to their dependency on preparation conditions and the type and quantity of dopants[16]. Accordingly, attempt has been in this current research work to study the dielectric properties of as prepared $Cu_{0.2}Zn_{0.8}Fe_2O_4$, $Cu_{0.6}Zn_{0.4}Fe_2O_4$ and $Cu_{0.8}Zn_{0.2}Fe_2O_4$ samples.

2.0 Experimental Methods

2.1 Sample Preparation and XRD Studies

The samples were prepared through an auto combustion route. Nitrates of the required metals, copper, zinc and iron were weighted stoichiometrically and mixed with citric acid in deionized water. The solution was then transferred to a preheated furnace at 450° C in a crucible for combustion process. After combustion a foamy powder was obtained. The as obtained sample was grinded to fine powder and further calcinated at 1000° C. X-Ray Diffraction (XRD) plots of the samples were obtained using Rigaku Smart lab to verify crystal formation and phase purity.

2.2 Impedance Spectroscopy Studies

The electrical impedance analysis is carried out by applying an alternating sinusoidal voltage to the sample that is

investigated and measuring the *ac* current response. The investigated powder sample is first converted into a pellet by applying hydraulic pressure of 5 tons, and then silver paste contacts are made to both circular cross-sections of the pellet, and copper wires are attached to this silver paste contacts. Silver is chosen in making the contacts due to its high conductivity. These contacts are then kept for annealing at 100°C in the oven for ~12 hours. In the present study, Agilent 4294A impedance analyzer, which is based on the auto-balanced bridge Implementation, is used. The samples under study were scanned from 40 Hz to 20 MHz at room temperature (300 K).

3.0 Results and Discussion

3.1 XRD Studies

XRD diffraction pattern of $Cu_{0.2}Zn_{0.8}Fe_2O_4$, $Cu_{0.6}Zn_{0.4}Fe_2O_4$ and$Cu_{0.8}Zn_{0.2}Fe_2O_4$ are presented in Figure 1. Peaks with planes (220), (311), (222), (400), (422), (511), (440) were identified correspondingly at 2θ positions 29.9, 35.2, 36.8, 42.9, 53.2, 56.7, and at 62.3 according to ICSD database with reference code 01-077-0012 of copper zinc iron oxide. This corresponds to cubic structure with space group *Fd-3m*[17]. The crystallite size of the samples

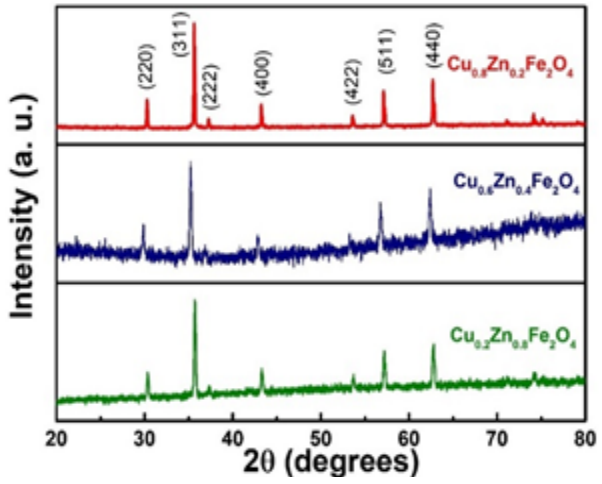

Figure 1. XRD spectra of $Cu_x Zn_{1-x} Fe_2 O_4$ (x = 0.2, 0.6, 0.8) samples.

was estimated using the Debye Scherrer method and was found to be in the range 37 to 47 nm.

3.2 Complex Dielectric Constant

Unlike in a vacuum, the frequency of external fields greatly influences how typical materials react to them. This frequency dependence highlights the fact that the polarization of a material does not change instantly when an electric field is applied. A phase difference can be used to represent the response, which must always be correlational (arising after the applied field). As a result, permittivity is frequently modeled as a complex function of the applied field's (angular) frequency. The complex dielectric constant can be written as a sum of real and imaginary part as given by

$$\varepsilon^*(\omega) = \varepsilon'(\omega) + i\varepsilon''(\omega) \qquad (1)$$

Both real and imaginary parts of the complex dielectric constant were calculated as per the equations shown below for the complex impedance[18].

$$\varepsilon' = \frac{t}{A\omega\varepsilon_0}\frac{Z'}{Z'^2 + Z''^2} \qquad (2)$$

$$\varepsilon'' = \frac{t}{A\omega\varepsilon_0}\frac{Z''}{Z'^2 + Z''^2} \qquad (3)$$

Where t is the thickness of the pellet and A is the cross-sectional area of the pellet. Z' and Z"correspond to real and imaginary parts of impedance. The variation of both the real and imaginary parts of the complex dielectric constant with the frequency are shown in Figure 2.

Figure 2(a) shows the variation of the real part of dielectric constant ($\dot{\varepsilon}$) of $Cu_xZn_{1-x}Fe_2O_4$ (x = 0.2, 0.6, 0.8) as a function of frequency. From the obtained plots we can clearly see that the values of dielectric constant are higher at lower frequencies and lower at higher frequencies. Maxwell type of polarization phenomena as well as Koop's phenomenological theory, which are in agreement with each other, can explain the variation of dielectric constant[19]. According to this theory, exchange of electrons between $Fe^{3+} - Fe^{2+}$ ascertain the applied electric field aiding polarization at lower frequencies. This leads to the variation of the values of dielectric constant ranging from higher value and slowly decreasing as the frequency is advancing. Higher frequencies, on the other

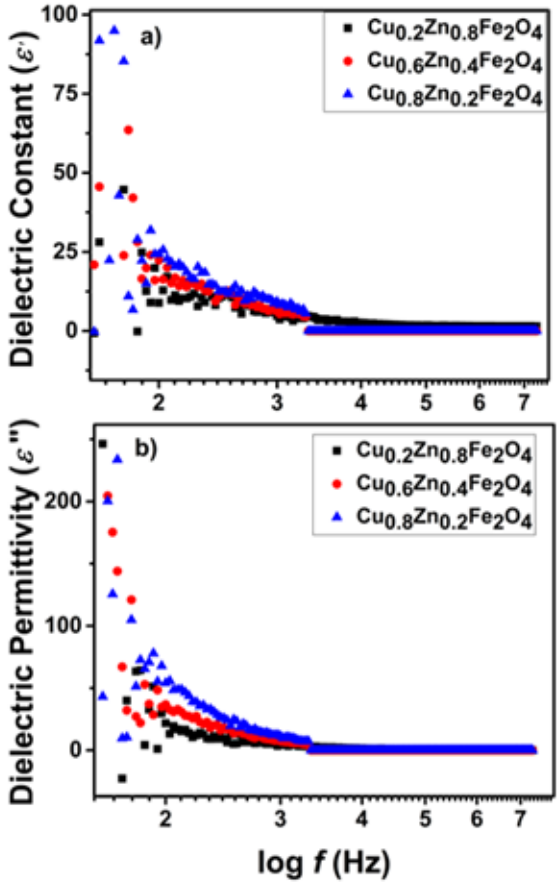

Figure 2. Variation of **(a)** dielectric constant (ε′) as a function of log(*f*), **(b)** dielectric permittivity (ε″) as a function of log (*f*) for the systems $Cu_xZn_{1-x}Fe_2O_4$ (x = 0.2, 0.6, 0.8).

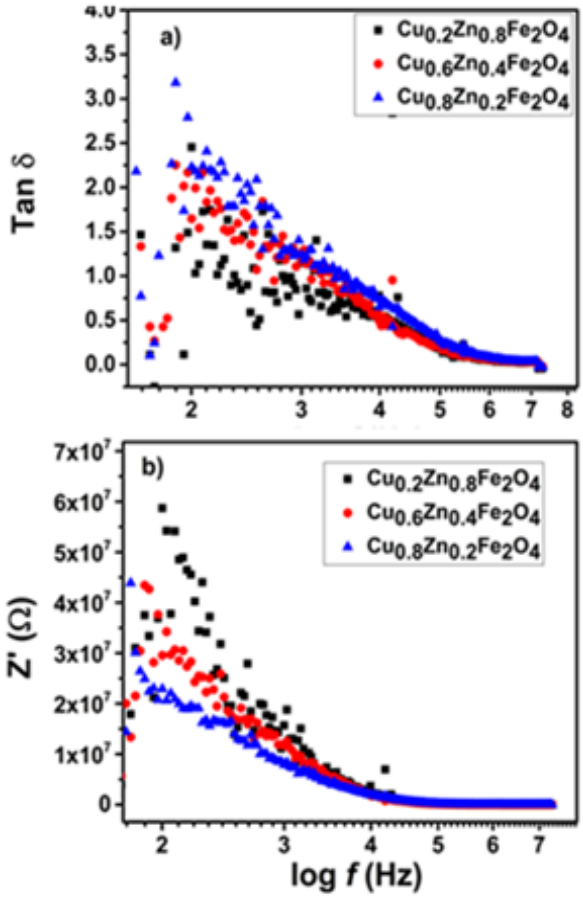

Figure 3. (a) The variation of dielectric loss tangent tan(δ) (b) Variation of real part of impedance (Z') of $Cu_xZn_{1-x}Fe_2O_4$ (x=0.2, 0.6, 0.8) as a function of frequency.

hand, prevent the electron exchange between Fe^{3+} and Fe^{2+} from tailing the applied electric field, which results in a lower dielectric constant value. Similar behavior and response we track for the variation of dielectric permittivity as a function of frequency.

3.3 Dielectric Loss Tangent (tan δ) and Impedance Measurements

The information about the energy dispersed inside materials as a result of impurities and defects is given by the dielectric loss tangent. The variation in stoichiometry, the Fe^{3+} content, and structural homogeneity all would affect the dielectric loss tangent. The loss tangent is additionally influenced by the conduction mechanism[20].

The decrease in energy observed in the ferrite is measured by the dielectric loss tangent, which is calculated using the formula,

$$\tan(\delta) = \frac{\varepsilon''}{\varepsilon'} \qquad (4)$$

The polarization trails the applied alternating field as the dielectric loss tangent grows. The graph of dielectric loss that varies with frequency is shown in Figure 3(a). The experimental finding shows that the dielectric loss factor is high for all the samples (studied in this work) in the lower frequency range. The existence of grain boundaries influences the dielectric loss. Due to the presence of grain boundaries, there is greater resistance, which causes significant dielectric

loss. Transport of electrons between Fe^{3+} and Fe^{2+} ions require sufficient energy at lower frequency, resulting in significant dielectric loss. However, because of grains, the resistivity decreases in high frequency regions[21]. The electron transport mechanism between the two iron ions requires only a little amount of energy at the octahedral sites.

Impedance spectroscopy connects the material's microstructures to its dielectric characteristics. Additionally, it aids in the analysis of the effects of numerous elements on polycrystalline materials, such as grain borders, interfaces, or grains. Impedance measurements statistically provide data concerning resistive and reactive components[22]. Figure 3b, the graph that represents real part impedance, shows fluctuation in the data as a function of frequency. The outcome of the experiment demonstrates that z' decreases with frequency.

3.4 AC Conductivity

The charge carrier and conduction mechanism in ferrite materials are explained by conductivity studies. The most frequent aspects affecting a material's conduction behavior include grain boundaries, mobility of charge carriers, space charge polarization, electron hopping, and particle size. The *ac* conductivity (σ_{ac}) is calculated using the following equation[18].

$$\sigma_{ac} = \frac{t}{A}\frac{Z'}{Z'^2 + Z''^2} \qquad (5)$$

Total conductivity σ_{tot} can be written as sum of σ_{dc} and σ_{ac} where the *dc* conductivity is, obviously, a frequency independent part of the total conductivity and is dominant in low frequency ranges, *ac* conductivity follows Jonscher's power law relation, and shows dispersive behavior at higher frequencies.

$$\sigma_{ac} = A' f^s \qquad (6)$$

Eqn. for σ_{ac} is the Jonscher's power law[23]. is the polarizability strength (temperature independent factor) and '*s*' represents exponent term and is temperature dependent factor, which gives significant information related to the theoretical model used to explain the conduction mechanism. The variation of *ac* conductivity

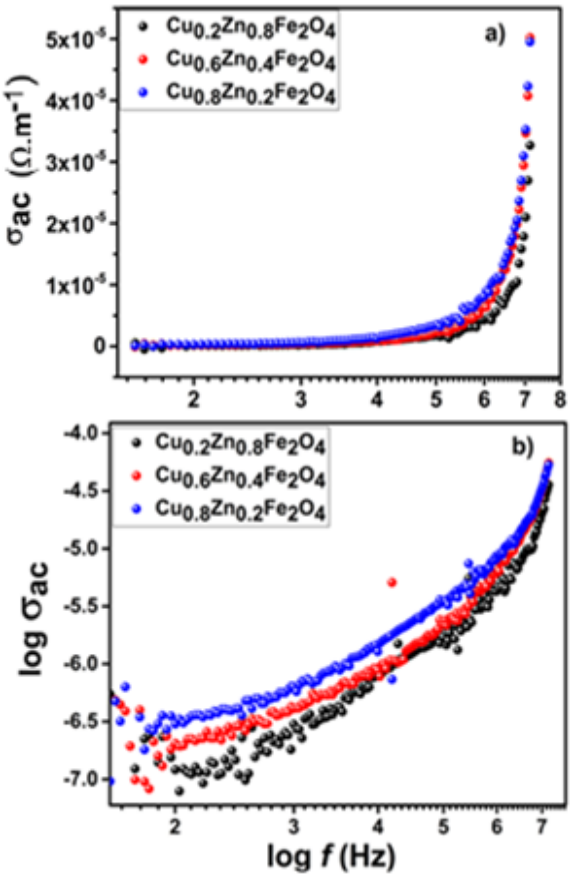

Figure 4. **(a)** Variation of σ_{ac} vs log (*f*) **(b)** variation of log (σ_{ac}) vs log (*f*) is given for samples $Cu_x Zn_{1-x} Fe_2 O_4$(*x*=0.2, 0.6, 0.8). The observed values of *s* are less than 1 supporting hopping mechanism.

(σ_{ac}) as a function of frequency of $Cu_xZn_{1-x}Fe_2O_4$(*x* = 0.2, 0.6, 0.8) is shown in Figure 4. From the Figure it is evident that conductivity slowly increases at the low frequency region, whereas at the higher frequency region, conduction starts increasing exponentially, which could be attributed to the hopping of infinite charge carriers.

Koop's phenomenological theory[24] explains the variation in conductivity as a function of frequency quite well. This theory not only explains the mechanism of higher frequency conductivity, but also sheds light on the material aspects. Grain boundaries and grains make up a material or compound. The material's high conductivity is attributable to grains, while its low conductivity is directly

attributable to grain boundaries. At lower frequencies, grain boundaries cope with the applied frequency, resulting in higher resistance and constant conductivity. However, at higher frequencies, grain boundaries have less of an effect and grains aid in conductivity. As a result, conductivity increases exponentially at higher frequencies. In this case, charge carriers hop between adjacent sites, resulting in increased conductivity. Thus, the highly resistive grain boundaries become irrelevant at higher frequencies, and hence the conductivity increases.

3.5 Cole-Cole Plot (Nyquist Plots)

Complex impedance spectrum (Cole-Cole) plots of the samples are demonstrated in Figure 5. From these spectra we can acquire information regarding conduction mechanism and charge transport properties of the materials under study. This indicates a non-Debye type of relaxation since we see dispersion on the real axis unlike a centered semicircle[25]. According to previous work on ferrites[26], researchers have observed two distinct semi circles related to compounds under study. The first one, at low frequency region, is associated with resistance due to grain boundary, whereas one observed at high frequency refers to resistance due to grains. Impedance spectroscopic study is able to distinguish this both because relaxation times of grains and grain boundaries are distinct[3]. In the present investigation, we have observed an individual semicircle minor arc, demonstrating conduction due to grains is dominant in the systems copper doped zinc ferrites. Since all the measurements are done at room temperature in the present study, they may not necessarily be well resolved. Moreover, in grain boundaries transport properties are also associated with presence of imperfections which could be more predominant than grains.

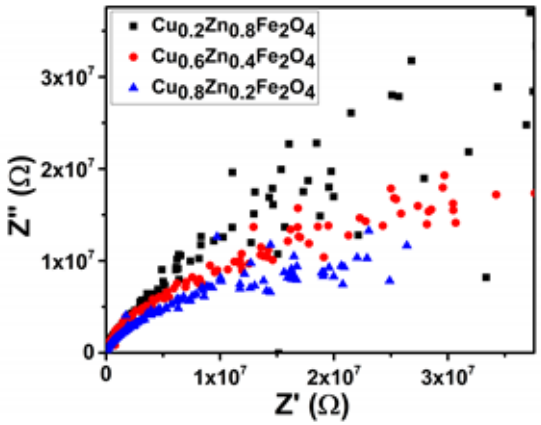

Figure 5. Cole-Cole plot of $Cu_xZn_{1-x}Fe_2O_4$ (x = 0.2, 0.6, 0.8) samples at room temperature.

4.0 Conclusion

$Cu_xZn_{1-x}Fe_2O_4$ (x = 0.2, 0.6, 0.8) samples were successfully prepared through auto combustion route. From XRD analysis homogeneous phase formation of spinel structure with space group Fd-3m was verified. The compositional dependence of electrical parameters was investigated using impedance spectroscopy technique. The observed dielectric behavior is in agreement with Koop's theory and loss tangent impedance variance are concluded to be due to exchange interaction, presence of grains and interfaces. In complex impedance spectrum a non-Debye type of relaxation was observed showing conduction is mostly mediated by grains. The practical deployment of Zn-doped $CuFe_2O_4$-based gas sensors in the mining industry will greatly increase safety, lessen environmental effect, and boost overall mining operations efficiency. This shift in dielectric characteristics can be utilized for this purpose.

5.0 Acknowledgement

Brian Jeevan Fernandes wishes to thank the University Grant Commission, Govt of India, for Dr. D S Kothari Post-Doctoral Fellowship. K. J. M. gratefully acknowledges financial support, as seed money grant (2022/1010), received from the Gokula Education Foundation (M), Bengaluru, India.

6.0 References

1. Zaki HM, Al-Heniti SH, Elmosalami TA. Structural, magnetic and dielectric studies of copper substituted nano-crystalline spinel magnesium zinc ferrite. J Alloys Compd. 2015; 633:104–14. https://doi.org/10.1016/j.jallcom.2015.01.304

2. Manjunatha M, Reddy GS, Mallikarjunaiah KJ, Ramesh KP. Effect of aluminium substitution in magnetically affluent inverse spinel ferrites studied via ^{57}Fe-Internal field NMR. J Mol Struct. 2020 Jun 5; 1209. https://doi.org/10.1016/j.molstruc.2020.127956
3. Mujasam Batoo K. Study of dielectric and impedance properties of Mn ferrites. Physica B Condens Matter. 2011; 406(3):382–7. https://doi.org/10.1016/j.physb.2010.10.075
4. Amin N, Hasan MS, Majeed Z, Latif Z, un-Nabi MA. Structural, electrical, optical and dielectric properties of yttrium substituted cadmium ferrites prepared by Co-Precipitation method. Ceram Int. 2020; 46(13):20798–809. https://doi.org/10.1016/j.ceramint.2020.05.079
5. Kaur M, Kaur N, Vibha. Ferrites: Synthesis and Applications for Environmental Remediation. In: ACS Symp Ser Am Chem Soc. 2016; 113–36. https://doi.org/10.1021/bk-2016-1238.ch004
6. Ghodake UR, Chaudhari ND, Kambale RC, Patil JY, Suryavanshi SS. Effect of Mn^{2+} substitution on structural, magnetic, electric and dielectric properties of Mg-Zn ferrites. J Magn Magn Mater. 2016; 407:60–8. https://doi.org/10.1016/j.jmmm.2016.01.022
7. Tahir Farid HM, Ahmad I, Ali I, Mahmood A, Ramay SM. Structural and dielectric properties of copper-based spinel ferrites. Eur Phys J Plus. 2018; 133(2). https://doi.org/10.1140/epjp/i2018-11832-4
8. Dutrizac JE. The leaching of sulphide minerals in chloride media. Hydrometallurgy. 1992; 29. https://doi.org/10.1016/0304-386X(92)90004-J
9. Wang, Weixing, Zhenghe X, J. Finch. Fundamental study of an ambient temperature ferrite process in the treatment of acid mine drainage. Environ Sci Technol. 1996; 30(8):2604–8. https://doi.org/10.1021/es960006h
10. Igarashi T, Herrera PS, Uchiyama H, Miyamae H, Iyatomi N, Hashimoto K, *et al*. The two-step neutralization ferrite-formation process for sustainable acid mine drainage treatment: Removal of copper, zinc and arsenic, and the influence of coexisting ions on ferritization. Sci Tot Environ. 2020; 715. https://doi.org/10.1016/j.scitotenv.2020.136877
11. Chapelle A, El Younsi I, Vitale S, Thimont Y, Nelis T, Presmanes L, *et al*. Improved semiconducting CuO/$CuFe_2O_4$ nanostructured thin films for CO_2 gas sensing. Sens Actuators B Chem. 2014; 204:407–13. https://doi.org/10.1016/j.snb.2014.07.088
12. Haija MA, Ayesh AI, Ahmed S, Katsiotis MS. Selective hydrogen gas sensor using $CuFe_2O_4$ nanoparticle based thin films. Appl Surf Sci. 2016; 369:443–7. https://doi.org/10.1016/j.apsusc.2016.02.103
13. Ranjith Kumar E, Siva Prasada Reddy P, Sarala Devi G, Sathiyaraj S. Structural, dielectric and gas sensing behavior of Mn substituted spinel MFe_2O_4 (M=Zn, Cu, Ni, and Co) ferrite nanoparticles. J Magn Magn Mater. 2016; 398:281–8. https://doi.org/10.1016/j.jmmm.2015.09.018
14. Verma K, Kumar A, Varshney D. Effect of Zn and Mg doping on structural, dielectric and magnetic properties of tetragonal $CuFe_2O_4$. Curr Appl Phys. 2013; 13(3):467–73. https://doi.org/10.1016/j.cap.2012.09.015
15. Cutmore NG, Liu Y, Middleton AG. ore characterization and sorting. Miner Eng. 1997; 10(4):421-6. https://doi.org/10.1016/S0892-6875(97)00018-6
16. Zaki HM. Temperature dependence of dielectric properties for copper doped magnetite. J Alloys Compd. 2007; 439(1–2):1–8. https://doi.org/10.1016/j.jallcom.2006.08.084
17. Karanjkar MM, Tarwal NL, Vaigankar AS, Patil PS. Structural, Mössbauer and electrical properties of nickel cadmium ferrites. Ceram Int. 2013; 39(2):1757–64. https://doi.org/10.1016/j.ceramint.2012.08.022
18. Joshi JH, Kanchan DK, Joshi MJ, Jethva HO, Parikh KD. Dielectric relaxation, complex impedance and modulus spectroscopic studies of mix phase rod like cobalt sulfide nanoparticles. Mater Res Bull. 2017; 93:63–73. https://doi.org/10.1016/j.materresbull.2017.04.013
19. Manjunatha K, Jagadeesha Angadi V, Jeevan Fernandes B, Parthasarathy Ramesh K. Synthesis and Study of Structural and Dielectric Properties of Dy-Ho Doped Mn-Zn Ferrite Nanoparticles. In: Ferrites - Synthesis and Applications. Intech Open. 2021. https://doi.org/10.5772/intechopen.99264
20. Bhoyar DN, Somvanshi SB, Nalle PB, Mande VK, Pandit AA, Jadhav KM. Multiferroic Fe^{3+} ion doped $BaTiO_3$ perovskite nanoceramics: Structural, optical, electrical and dielectric investigations. In: Journal of Physics: Conference Series. IOP Publishing Ltd; 2020. https://doi.org/10.1088/1742-6596/1644/1/012058
21. Iwauchi K. Dielectric properties of fine particles of Fe_3O_4 and some ferrites. Japanese Journal of Applied Physics. 1971; 10(11):1520. https://doi.org/10.1143/JJAP.10.1520
22. Khan SB, Irfan S, Lee SL. Influence of Zn^{+2} doping on ni-based nanoferrites; ($Ni_{1-x} Zn_x Fe_2O_4$). Nanomater. 2019; 9(7). https://doi.org/10.3390/nano9071024

23. Lukichev AA. Nonlinear relaxation functions. Physical meaning of Jonscher's power law. J Non Cryst Solids. 2016; 442:17–21. https://doi.org/10.1016/j.jnoncrysol.2016.02.027
24. Koops CG. On the Dispersion of Resistivity and Dielectric Constant of Some Semiconductors at Audiofrequencies. Phys Rev. 1951; 83. https://doi.org/10.1103/PhysRev.83.121
25. Hegde SS, Jeevan Fernandes B, Talapatadur V, Ramesh KP, Ramesh K. Impedance spectroscopy analysis of SnS chalcogenide semiconductors. Mater Today Proc. 2022; 62:5648–52. https://doi.org/10.1016/j.matpr.2022.04.966
26. Gutierrez-Amador MP, Valenzuela R. Effects of grain size distribution on Cole-Cole plots of polycrystalline spinels. MRS Online Proceedings Library (OPL). 2001; 699. https://doi.org/10.1557/PROC-699-R3.1